ACS Catalysis

pubs.acs.org/acscatalysis

Research Article

Polymer Upcycling by Catalytic Hydrogenolysis: The Role of Polyolefin Short-Chain Branching

Zachary M. Gdowski, Rishi Raj, Aditya Bhan, K. Andre Mkhoyan, Mahesh K. Mahanthappa,* and Frank S. Bates*

Cite This: *ACS Catal.* 2025, 15, 16924−16937

Read Online

ACCESS | Metrics & More | Article Recommendations | Supporting Information

ABSTRACT: We report the hydrogenolysis of model short-chain branched polyolefins over a heterogeneous catalyst comprising 5−10 nm diameter Pt−Re nanoparticles supported on macroporous SiO_2 (0.1−1 μm pore diameters) to assess how polymer chain microstructure affects reactivity for upcycling applications. Living anionic homopolymerizations of 1,3-butadiene, isoprene, and styrene sometimes with a polar modifier followed by surface-catalyzed saturation afforded a series of narrow dispersity polyolefins with well-defined number-average molecular weights (M_n) and variable branch types and contents, including poly(ethylene-*co*-1-butene) copolymers (denoted hPB) with 1.5−38 ethyl branches per 100 backbone carbons, poly(ethylene-*alt*-propylene) (PEP), and poly(cyclohexylethylene) (PCHE). A model high-density polyethylene (HDPE) of comparable M_n with no short chain branches was also produced by tandem ring-opening metathesis polymerization and catalytic hydrogenation. Size-exclusion chromatography (SEC) analyses of the products of polymer hydrogenolysis in cyclohexane at T = 140−200 °C for ≤17 h over the Pt−Re/SiO_2 catalyst show that the amount of short chain branching impacts the extent of polymer cleavage. Specifically, M_n reductions of nearly 100-fold are achieved for HDPE and lightly branched hPB (1.5−10 branches per 100 backbone carbon atoms), 10-fold for PEP, and less than 2-fold for the highly branched hPB and PCHE. These strong correlations between branching and susceptibility to hydrogenolysis in polyolefins have important implications for the ability to upcycle waste single-use hydrocarbon polymers and their mixtures.

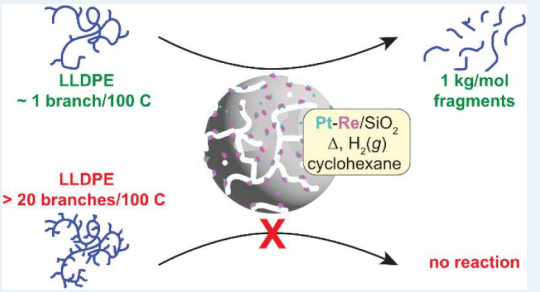

KEYWORDS: *polyolefin hydrogenolysis, polymer upcycling, recycling, sustainability, plastic degradation*

Downloaded via UNIV OF MINNESOTA on May 8, 2026 at 00:35:39 (UTC).
See https://pubs.acs.org/sharingguidelines for options on how to legitimately share published articles.

INTRODUCTION

Polyolefins such as polyethylene (PE) and polypropylene (PP), which represent a majority of the single-use plastic produced worldwide, are a substantial component in the global plastic waste problem.[1−4] One potential means of addressing this issue is to chemically decompose or "upcycle" these relatively chemically inert polymers into useful low molecular weight products for reuse in other applications.[5−7] Hydrogenolysis is an especially attractive catalytic upcycling process, wherein carbon−carbon bond cleavage by the addition of hydrogen converts the initial high molecular weight hydrocarbon polymers into value-added lower molecular weight compounds such as lubricants and fuel-range hydrocarbons.[8−10] Over the past few years, a wealth of publications have examined the hydrogenolysis of commercial grade polyolefins using various heterogeneous transition metal catalysts, addressing the roles of the active metal,[11−15] support architecture,[14−19] and other reaction conditions[13,16,19−35] to address the upcyclability of various commercial and post-consumer plastic waste streams.[12−15,20−23,34,36−49]

In catalytic refining of crude oil into liquid hydrocarbon reformates, bimetallic Pt−Re catalysts supported on inorganic oxide supports (e.g., SiO_2 and Al_2O_3) have long been used for catalytic cracking, dehydrogenation, and hydrogenation reactions.[50−54] Pt−Re/Al_2O_3 modified catalysts are used industrially for naphtha reforming, with alloying characteristics and promoters (Cl, S) being added to maximize rates and limit hydrocracking. The addition of Pt is also known to facilitate reduction of ReO_x species at much lower temperatures relative to conditions where no Pt is present. The specific roles of Pt and Re in alkane hydrogenolysis are not known although it is plausible that the mechanisms are similar to those in naphtha reforming. We refer the interested reader to the extensive literature on bimetallic catalysts, notably work by Sinfelt and coworkers, which led to the development of currently employed Pt−Re reforming catalysts.[55−57]

Approximately 30 years ago, Hucul, Hahn and coworkers at the Dow Chemical Co.[58] realized the possibility of using such catalysts supported on ultrawide-pore mesoporous silicas for

Received: June 29, 2025
Revised: September 10, 2025
Accepted: September 15, 2025
Published: September 23, 2025

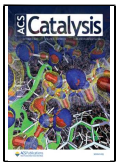

© 2025 American Chemical Society

https://doi.org/10.1021/acscatal.5c04494
ACS Catal. 2025, 15, 16924−16937

the complete hydrogenation of poly(styrene) to produce poly(cyclohexylethylene) (PCHE, sometimes called poly(vinylcyclohexane) or PVCH)[59−62] as a high glass transition temperature ($T_g \approx 140$ °C) and high modulus engineering thermoplastic with useful optical properties.[63,64] In order to effect this polymer saturation reaction in solution with commercially viable kinetics, they developed a precatalyst comprising Pt nanoparticles supported on islands of ReO_x in a macroporous silica support with 0.1−1 μm pore diameters.[58] The ultrawide-pore silica support is a key feature of this bimetallic catalyst, as it enables facile diffusion of solvated polymers into and out of the catalyst pores that gives rise to commercially useful hydrogenation kinetics. Addition of rhenium to the Pt-based catalyst improves resistance to catalyst deactivation during commercial application in polymer hydrogenation as documented in a patent disclosure.[64] Subsequent extension of this Pt−Re/SiO_2-catalyzed hydrogenation process to cyclohexane solutions of poly(styrene)/poly(butadiene) triblock and pentablock polymers is now a well-established route commercially practiced by USI Corp. for the production of poly(ethylene)/poly(cyclohexylethylene) copolymers, which are sold under the trade name ViviOn cyclic block copolymers.[65]

We and others have subsequently used this Pt−Re/SiO_2 catalyst (or a related catalyst with only Pt) for lab-scale hydrogenations of various model hydrocarbon polymers.[66−70] However, we found that substitution of $D_2(g)$ as the saturation reagent leads to catalytic hydrogen−deuterium (H/D) exchange of both backbone and side chain hydrogens of hydrocarbon polymers, including commercial grades of polyethylene and polypropylene. The extent of H/D exchange depends on polymer chemical identity and molecular weight, solvent, catalyst loading, and reaction temperature.[70−74] Experiments by Habersberger et al. demonstrated exchange of 32−68% of hydrogen for deuterium atoms on a commercial HDPE reacted over the Pt−Re/SiO_2 catalyst in hydrocarbon solvents.[71] SEC-IR measurements showed that the extent of exchange differed significantly across the broad polymer molecular weight distribution.[72] Zeng et al. and Kang et al. reported nonmonotonic trends regarding isotopic exchange as a function of side chain branch density,[70,73] and Zeng et al. demonstrated that deuterium exchange in hydrogenated polybutadienes resulted in preferential exchange with side chain versus backbone hydrogen atoms.[70] Here, we note that these previous works were conducted without any catalyst activation by heat treatment under vacuum that impacts catalyst reactivity (see below).

More recently, Ertem et al. noted that Pt−Re/SiO_2 also effects limited degrees of polymer backbone cleavage at 170 °C under 500 psig $D_2(g)$ at high catalyst loadings (1:1 *w*/*w* polymer:catalyst) over 17 h.[75] Those studies indicated that solutions of polystyrene (PS) and high-density PE (HDPE) in isooctane did not degrade when reacted with Pt−Re/SiO_2 under $D_2(g)$, yet poly(ethylene-*alt*-propylene) (PEP) was reduced to half its starting molecular weight, and commercial linear low-density PE (LLDPE) was degraded to roughly 5% of its initial molar mass. These seemingly inconsistent results suggest that solution hydrogenolysis over this bimetallic catalyst depends on the type and distribution of pendant groups along the carbon backbone, consistent with the trends observed for H/D exchange as a function of side chain content.[70,73] Also, Ertem et al. found that the analogous Pt/SiO_2 catalyst, i.e., without Re, was much less active in LLDPE hydrogenolysis. Ultimately, the detailed atomic structures of these catalysts and the mechanisms by which Pt and Re synergistically act remain obscure due to the limited resolution of available characterization methodsrelevant to examine catalysts under working conditions, despite years of research.[55−57]

Here, we report experiments based on the series of model polyolefin materials depicted in Figure 1 that explicitly address

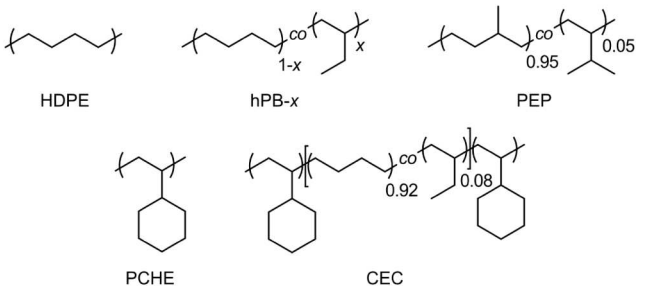

Figure 1. Model polyolefins subjected to cyclohexane solution hydrogenolyses over a Pt−Re/SiO_2 catalyst. For the hPB samples, the branch content varies with $0.06 \leq x \leq 0.86$.

the impact of chain microstructure on cyclohexane solution hydrogenolysis reactions catalyzed by Pt−Re/SiO_2 at $140 \leq T \leq 200$ °C under 500 psig $H_2(g)$. In order to assess how the density of short chain branching influences LLDPE degradation, our model substrates include a series of hydrogenated polybutadienes (hPBs) with narrow molar mass dispersities and 1.5−38 ethyl branches per 100 backbone carbon atoms ($0.06 \leq x \leq 0.86$ in Figure 1). Additionally, we evaluated the extent of chain cleavage under these reaction conditions for a model HDPE, poly(ethylene-*alt*-propylene) (PEP), PCHE, and a commercial PCHE-*block*-PE-*block*-PCHE (CEC) triblock polymer. Apart from the model HDPE sample, these model polyolefins were derived from a tandem sequence of anionic polymerization and catalytic hydrogenation. We document polymer degradation ranging from virtually no change (PCHE) to a 100-fold reduction (hPB-06) in molecular weight depending on the type and density of side chains in the starting materials. These findings will aid in the design and scale-up of upcycling processes for converting a wide spectrum of commercially available polyolefins and their mixtures into useful low molecular weight chemical feedstocks.

EXPERIMENTAL METHODS

Materials. 1,3-Butadiene (99%, Sigma-Aldrich) was twice stirred over dry *n*BuLi at −20 °C for 1 h and distilled under vacuum prior to use. Isoprene (99%, Sigma-Aldrich) was analogously purified by twice stirring over dry *n*BuLi at 0 °C and distilling under vacuum. Styrene (99%, Sigma-Aldrich) was stirred and vacuum distilled at 40 °C from CaH_2, followed by twice vacuum distilling from *n*Bu(Et)Mg. *cis*-Cyclooctene (95%, Acros Organics) was filtered through basic alumina prior to use. Anhydrous toluene was obtained from a Glass Contour Inc. solvent purification system, while anhydrous cyclohexane (CHX) and tetrahydrofuran (THF) were obtained from an in-house purification system by passage through activated alumina and a Q5 deoxygenation catalyst.[76] This THF was further purified by vacuum distillation from BuMgCl at ambient temperature. All other reagents were used as received. The CEC triblock copolymer, with M_n = 35 kg/mol, $Đ$ = 1.02,

https://doi.org/10.1021/acscatal.5c04494
ACS Catal. 2025, 15, 16924−16937

and 62 wt % PCHE and 2.1 branches per 100 backbone carbons in the PE segment,[77] was acquired from the Dow Chemical Company (this material is presently sold by the USI Corp., Taipei, Taiwan).[65]

Model Polydiene Library Synthesis. Air- and water-free anionic polymerizations were performed on a Schlenk line under an argon atmosphere per established procedures, with the detailed reagent amounts reported in Table S1.[70] Poly(butadiene) (PB) with 94% 1,4 and 6% 1,2 repeat units (referred to as PB-06), was obtained by reaction of 1,3-butadiene with *s*BuLi in cyclohexane at 30 °C for 19 h. Polybutadienes with tailored amounts of 1,2-repeat units denoted PB-*x* ($0.33 \leq x \leq 0.86$) were synthesized from reaction of 1,3-butadiene with *n*BuLi in cyclohexane at 8 °C for up to 20 h in the presence of THF as a polar modifier with $2 \leq [\text{THF}]:[n\text{BuLi}] \leq 290$ (see Table S2 for details). Polymerizations were terminated by addition of degassed methanol. Polystyrene (PS) and polyisoprene (PI) were synthesized by anionic polymerizations in cyclohexane at 40 °C initiated with *s*BuLi and terminated by addition of either CH_3OH or slightly acidic CH_3OH (~100 μL 37% *w*/*w* hydrochloric acid in 20 mL of methanol).

Catalytic Hydrogenation of Model Polydienes. All polydiene hydrogenation reactions were carried out in a Parr 236HC 1 L reactor under 500 psig $H_2(g)$ with magnetic stirring by a Teflon stir bar. A solution of PB-06 (~5.5 g) in toluene (500 mL) was added to the 1 L reactor and sparged with Ar(*g*) for 30 min. The reactor was then vented, opened to the atmosphere, and 180 mg tris(triphenylphosphine)-rhodium(I) chloride (Wilkinson's catalyst) and 1.0 g triphenylphosphine were added. The sealed reactor was again sparged with Ar(*g*) for 30 min, pressurized with $H_2(g)$ to a static pressure of 500 psig, and heated to 100 °C for 12−20 h. The resulting polymer, which we designate hPB-06, was recovered by two or three precipitations from hot toluene (~90 °C) into cold methanol, which was accompanied by a change in polymer color from yellow-orange to white associated with removal of the catalyst. The resulting hPB-06 was dried at 50 °C under vacuum.

Since Wilkinson's catalyst is less effective for exhaustively hydrogenating PB-*x* with $x > 0.06$,[78] $Pd/CaCO_3$ (5 wt % Pd, reduced, Alfa Aesar) was used per a reported procedure[79] to hydrogenate the remaining PB-*x* samples. Briefly, the catalyst (~5 g, 1:1 *w*/*w* polymer) was dried under vacuum in the Parr reactor overnight at 100 °C followed by activation with 100 psig $H_2(g)$ at 100 °C for 1 h. Upon cooling to room temperature and venting the $H_2(g)$, a 1 wt % PB-*x* in cyclohexane solution (500 mL) was added to the reactor under dynamic Ar(*g*) pressure. The reactor was then pressurized to a static pressure of 500 psig $H_2(g)$ and reacted at 100 °C for 37−50 h, to produce hPB-*x*. PI was hydrogenated using an analogous procedure to produce poly(ethylene-*alt*-propylene) (PEP), and PS was similarly saturated at 120 °C to yield poly(cyclohexylethylene) (PCHE). Polymers were recovered by pressure-driven membrane filtration (~80 psig Ar(*g*) head pressure) through Fisherbrand P8 filter paper and a 0.22 μm Durapore membrane filter to remove the catalyst, followed by precipitation into −20 °C methanol. PEP and hPB-*x* polymers were dried under vacuum at 50 °C, and PCHE was vacuum-dried at 100 °C.

Reactions produced >99% saturation as assessed by ^{1}H NMR (see Figures S7, S8, S15, S18, and S21 for representative traces of hydrogenated samples); see below for specific characterization conditions.

Synthesis of hPB-0. Poly(cyclooctene) of a targeted molecular weight M_n = 100 kg/mol was synthesized by Ru-catalyzed ring-opening metathesis polymerization (ROMP) of cyclooctene in toluene in the presence of *cis*-4-octene as a chain transfer agent with [cyclooctene]:[*cis*-4-octene] = 900:1.[80,81] Cyclooctene (12 mL), toluene (5.5 mL), and *cis*-4-octene (16 μL, diluted in toluene) were added to a round-bottom flask and sparged with Ar(*g*) for 30 min, followed by addition of Grubbs second generation catalyst (G2, 8.2 mg) in 1 mL toluene. The reaction was then heated to 40 °C for 30 min, after which it was quenched with excess ethyl vinyl ether (100 μL). PCOE was precipitated twice from hot toluene (~90 °C) into CH_3OH to yield a white polymer (indicative of catalyst removal) that was dried under vacuum at 50 °C to remove residual solvent.

PCOE was hydrogenated to form "perfectly linear" poly(ethylene) (referred to as HDPE or hPB-0) as previously reported.[80] The ROMP reaction product was separated into two parts; ~25 vol % of the solution was set aside for molecular characterization of the unsaturated PCOE as previously described. The remainder of the ROMP reaction product was diluted with toluene to reduce the viscosity, and that solution of PCOE, G2, and ethyl vinyl ether in toluene (150 mL total volume) was added to a Parr 452HC 0.3 L reactor and placed under inert atmosphere by sparging with 80 psig Ar(*g*).

The reactor was then sealed, pressurized to 500 psig $H_2(g)$, and heated to 100 °C for 20 h. The resulting polymeric reaction product was isolated by two precipitations from hot toluene (~90 °C) into cold CH_3OH, followed by drying under vacuum at 50 °C. Note that the presence of ethyl vinyl ether in the hydrogenation reaction supresses undesired olefin metathesis side reactions of the G2 catalyst during Ru-catalyzed hydrogenation.[80]

Pt−Re/SiO_2-Catalyzed Hydrogenolysis Reactions. Cyclohexane solution hydrogenolysis reactions using the Pt−Re/SiO_2 catalyst provided by the Dow Chemical Co. were performed in the 0.3 L Parr reactor stirred with an "X"-shaped magnetic Teflon stir bar (Chemglass Inc., Vineland, NJ). 1.0 g of macroporous Pt−Re/SiO_2 catalyst was first dried under vacuum in the reactor overnight at 100 °C to remove organic impurities, as acetic acid was apparently used as a surface passivation agent possibly to reduce catalyst handling hazards. The reactor was then pressurized to 50 psig with Ar(*g*) and vented to ambient pressure for subsequent addition of 1.0 g polymer and 130 mL cyclohexane. Thus, the reaction is conducted with an approximately 1:1 *w*/*w* catalyst:polymer ratio. Semicrystalline polymers hPB-06, HDPE, and CEC, which are insoluble in cyclohexane at ambient temperature, were added as solids along with anhydrous cyclohexane (130 mL). hPB-33, hPB-60, hPB-61, hPB-86, PEP, and PCHE were dried overnight under vacuum at 22 °C, dissolved in anhydrous and anaerobic cyclohexane, and added to the reactor with additional solvent to achieve a total solution volume of 130 mL in each reaction. The reactor was sparged with 80 psig Ar(*g*) for 30 min, then pressurized to a static pressure of 500 psig $H_2(g)$ and allowed to react for 17 h at 140, 170, or 200 °C. Note that the reactor pressure decreases modestly over the course of the reaction (≤30% decrease from the initial pressure of 500 psig), but never fell below 300 psig. After 17 h, the reactor was cooled in an ice water bath to

https://doi.org/10.1021/acscatal.5c04494
ACS Catal. 2025, 15, 16924−16937

rapidly decrease its temperature to ambient temperature over the course of ∼5 min.

Hydrogenolytic degradation products obtained from the amorphous polymers hPB-33, hPB-60, hPB-61, hPB-86, PEP, and PCHE remained cyclohexane-soluble and were recovered by pressure-driven membrane filtration as in the polymer hydrogenation reactions. The hydrogenolysis products were subsequently isolated by cyclohexane removal by freeze-drying under vacuum. Note that precipitation of the reaction products was explicitly avoided to minimize loss of low molecular weight products. Hydrogenolysis of semicrystalline HDPE, hPB-06, and CEC instead produced a mixture of semicrystalline and amorphous polymer fragments with limited solubility in cyclohexane. In these cases, the cyclohexane was first removed by freeze-drying, followed by dissolution and hot filtration of the catalyst/polymer mixture in mixed xylenes at 130 °C to avoid crystallization-induced precipitation. The xylene solvent was removed by freeze-drying under vacuum at ambient temperature, and the resulting solid materials were further dried at either 100 °C (for PCHE and CEC) or 50 °C (for all other species) to remove any residual solvent.

For selected samples, up to four replicate hydrogenolysis batch reactions were performed to assess reaction reproducibility. Batch reactions using the same conditions were also performed, wherein aliquots (≈20 mL) were taken at specified time intervals to monitor the time course of catalytic chain scission reactions. Details regarding the time sampling reactions are provided in Supporting Information, along with a photograph of the sampling apparatus (Figure S1).

Size Exclusion Chromatography (SEC). Initial model polyolefin and hydrogenolysis reaction product molecular weights were determined by high-temperature size-exclusion chromatography (HT-SEC) in 1,2,4-trichlorobenzene (TCB, stabilized with 0.02 wt % butylated hydroxytoluene) at 135 °C with a flow rate of 1 mL/min. These analyses employed an Agilent PL-GPC 220 SEC system equipped with three PL-Gel Mixed B columns, a differential refractive index (RI) detector, and a Wyatt DAWN HELEOS II LS 18-angle detector for absolute molecular weight quantification. Samples were prepared with concentrations of 1−4 mg polymer/mL of filtered TCB. Light scattering analyses used the refractive index increment dn/dc values for the samples in TCB at 135 °C or a 100% mass recovery assumption for samples where literature values of dn/dc were not available. Alternatively, a Mark−Houwink (M−H) corrected calibration curve based on tabulated values of the M−H constants K and a in TCB at 135 °C was constructed from a conventional calibration curve derived from analyses of narrow dispersity polystyrene standards with M_n = 500−123 000 g/mol.

Nuclear Magnetic Resonance (NMR) Spectroscopy. ^{1}H NMR measurements were performed on a 500 MHz Bruker Avance III instrument using a 20 s pulse repetition delay with 16 transients in $CDCl_3$ for PS and PCHE, or in toluene-d_8 for all other polymers. Samples were prepared with a polymer concentration of ∼10 mg/mL and run at 27 °C. In the case of polymers not soluble at 27 °C, spectra were acquired at 90 °C.

^{13}C NMR spectra were acquired using an inverse-gated ^{1}H decoupled 30° pulse sequence performed with either a 2 or 6 s relaxation delay with >700 scans. For hPB samples, 5 wt % polymer solutions were prepared in 90/10 v/v 1,2-dichlorobenzene/1,1,2,2-tetrachloroethane-d_2 with 0.01−0.02 M chromium(III) acetylacetonate as a spin−lattice relaxation (T_1) agent that also minimizes impacts of the nuclear Overhauser Effects (NOEs).[82] Samples were measured at either 130 or 27 °C. For PCHE samples, 15 wt % polymer solutions were prepared in 90/10 v/v 1,2-dichlorobenzene/1,1,2,2-tetrachloroethane-d_2 with 0.03 M chromium(III) acetylacetonate and measured at 27 °C.

Differential Scanning Calorimetry (DSC). DSC measurements were conducted with a TA Instruments Q1000 instrument. Samples were heated and cooled at 10 °C/min, with crystallization temperature (T_c) values reported on first cooling, and glass transition and melting temperature (T_g and T_m) values reported on second heating. Data analyses were performed using the TA Universal Analysis software.

Gas Chromatography/Mass Spectrometry. Gas chromatography/mass spectrometry (GC/MS) measurements were performed using a Hewlett-Packard HP-6890 Series GC/QTOF-MS with helium carrier gas. The system was equipped with an Agilent 19091S-133 separation column and an electron impact ionization system. 2 μL of solution was manually injected into the instrument with a separation sequence involving a temperature ramp from 50 to 290 °C at a rate of 12 °C/min with no solvent delay.

A gas chromatography/flame ionization detection measurement was acquired using manual injection of 0.5 μL of sample into an S/SL inlet at 250 °C with a split ratio of 100. The sample was separated by an HP-PlotQ column, and the FID was set at 400 °C with H_2, air, and He makeup flows of 40 mL/min, 350 mL/min, and 20 mL/min, respectively. The temperature program involved holding at 40 °C for 3 min, followed by ramping to 270 °C at 20 °C/min and holding at 270 °C for 10 min.

Catalyst Characterization. Samples for scanning transmission electron microscopy (STEM) studies were prepared using a focused-ion beam (FIB) performed on an FEI Helios NanoLab G4 dual-beam system. The FIB was operated with a Ga-ion beam at 30 kV and an electron beam at 5 kV. An amorphous carbon (am-C) layer of ∼50 nm was deposited on the sample as a protective layer prior to FIB milling. Additional 1 μm protective layers of am-C and Pt were deposited on the region of interest. Another set of specimens was prepared by grinding the Pt−Re/SiO_2 catalyst powder into fine particles using a mortar pestle and drop casting from deionized water on a standard Cu TEM grid with am-C support. The specimens were investigated with a ThermoFisher Scientific Talos F200X STEM equipped with a Super-X energy dispersive X-ray (EDX) spectrometer. The microscope was operated at 200 kV with a probe convergence angle of 10.4 mrad and current of 80 pA. Images were acquired with detector inner and outer collection of angles of 46 and 200 mrad, respectively. The STEM-EDX elemental maps were analyzed with ThermoFisher Scientific Velox software. Experimental details for nitrogen adsorption isotherms and X-ray photoelectron spectroscopy measurements are provided in the SI.

RESULTS AND ANALYSIS

Pt−Re/SiO_2 Catalyst Characterization. Despite the extensive use of Pt/SiO_2 and Pt−Re/SiO_2 catalysts for polymer hydrogenations over the past 25 years, minimal characterization is available for these two hydrogenation catalysts developed by the Dow Chemical Co., including no published images of the Pt−Re/SiO_2 catalyst. Bates et al. reported transmission electron microscopy (TEM) and scanning electron microscopy (SEM) images of the Pt/SiO_2 catalyst,

https://doi.org/10.1021/acscatal.5c04494
ACS Catal. 2025, 15, 16924−16937

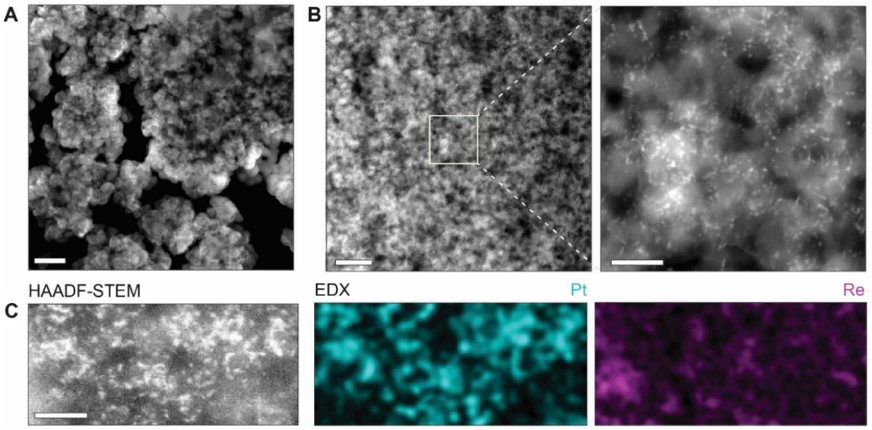

Figure 2. (A) Low-magnification HAADF-STEM image of Pt−Re/SiO_2 showing the macroporous silica morphology, where the scale bar is 250 nm. (B) Magnified HAADF-STEM image of Pt−Re/SiO_2 shown in (A). High-magnification image from the boxed area is shown on the right. Bright spots correspond to Pt−Re nanoparticles distributed within the SiO_2 matrix. Scale bars are 200 and 50 nm, respectively. (C) HAADF-STEM and corresponding EDX elemental maps showing the presence of Pt and Re nanoparticles distributed in the SiO_2 matrix, where the scale bar is 50 nm.

which exhibited ∼10 nm Pt nanoparticles grafted on a macroporous SiO_2 substrate.[63] In addition, Hucul and Hahn reported the development of the ultrawide-pore SiO_2 network that is used as the support in these two catalysts, wherein the average pore diameter is ∼0.4 μm as calculated from mercury porosimetry, upon which Pt−Re (or Pt) nanoparticles are deposited.[58]

We obtained high-angle annular dark-field scanning transmission electron microscopy (HAADF-STEM) images to better understand the catalyst structure and the associated length scales relative to the size of individual polymer chains in solution. The catalyst was first dried overnight at 100 °C under vacuum to mimic the procedure used for hydrogenolysis reactions, prior to preparation for imaging using a FIB lift-out technique. STEM images presented in Figure 2A,B clearly show the presence of a macroporous SiO_2 network, with pores and cavities >0.1 μm in size, consistent with prior reports of an average pore diameter of ∼0.4 μm based on mercury porosimetry measurements.[58,64] At higher resolution (inset panel in Figure 2B), Pt−Re nanoparticles are observed as bright spots with an average particle size of 3.3 nm, calculated from 2D line scans at five different locations in the micrograph (see Figure S2); note that the oxidation state of the metals cannot be discerned by this technique. While the nanoparticles are largely isolated, a fraction of the particles exist as agglomerates, suggesting a heterogeneous reaction environment.

Energy-dispersive X-ray (EDX) mapping using STEM was also performed on a separate sample prepared by pulverization and solvent drop-casting to avoid analysis errors stemming from additional Pt deposition during sample preparation. This analysis, shown in Figure 2C, shows the presence of both Pt and Re, albeit the Re signal is fainter and appears more broadly distributed than Pt. The EDX maps with the addition of the Si signal are provided in Figure S3A, and fitting of the spectra in Figure S3B indicates the presence of well-dispersed Pt and Re on the macroporous SiO_2 network, at roughly a 2 to 1 ratio of [Pt]:[Re].

The catalyst surface area was determined using a nitrogen adsorption isotherm. The corresponding Brunauer−Emmett−Teller (BET) plot (Figure S4) produced a surface area of 61.0 ± 0.7 m^2/g, consistent with a previous report on the Pt−Re/SiO_2 catalyst.[64] X-ray photoelectron spectra (XPS) were obtained (Figure S5), from which the surface composition was estimated as given in Tables S3 and S4. These results indicate surface atomic ratios of 10:1 for Pt:Re and 2.7:1 for O:Si. The platinum peak position corresponds to metallic Pt,[83] while the rhenium peak position is consistent with Re_2O_7, showing an oxidized rhenium state in the *ex situ* XPS experiment prior to treatment with $H_2(g)$.[84,85]

Model Polyolefin Synthesis and Characterization. Organolithium-initiated anionic polymerization of butadiene proceeds by either 1,4- or 1,2-addition pathways, with variations in solvent and temperature determining the final polymer microstructure.[86] Five hPBs with different microstructures were synthesized by anionic polymerization and subsequent hydrogenation with either Wilkinson's catalyst or Pd/$CaCO_3$ and characterized using NMR, SEC, and DSC. Molecular characteristics for these polymers are presented in Table 1 (see Figure 1 for chemical structures), with additional details given Figures S6−S14, Tables S1−S2 and S5. In brief, all polymers exhibit relatively low dispersities ($Đ = M_w/M_n$) and unimodal molecular weight distributions, calculated using SEC with multiangle light scattering and known differential refractive index increment values (dn/dc) for hPB in 1,2,4-trichlorobenzene (TCB).[87] The ethyl branch contents in the hPBs were determined based on the fraction of 1,2-repeat units in the unsaturated precursors determined by ^{1}H NMR. A semicrystalline polymer melting peak at T_m = 108 °C is evident in the DSC trace for hPB-06 (Figure S13), while all other hPB specimens exhibit no measurable crystallinity and display glass transitions at reduced temperatures (T_g < −10 °C, Figure S13).

Four other polymers were synthesized or acquired to better understand the impact of short-chain branches on polymer degradation: high-density polyethylene (HDPE), poly(ethylene-*alt*-propylene) (PEP), poly(cyclohexylethylene) (PCHE), and CEC, a triblock copolymer from the Dow Chemical Co. containing 62 wt % PCHE end blocks and a hydrogenated (1,4-rich) polybutadiene midblock (CEC).[77] Characterization data for these polymers are also provided in Table 1 (and Figures S15−S26 and Table S1), along with their chemical structures in Figure 1.

https://doi.org/10.1021/acscatal.5c04494
ACS Catal. 2025, 15, 16924−16937

Table 1. Model Polyolefin Molecular Characteristics Prior to Hydrogenolysis

Polymer[a]	M_n (kg/mol)[b]	$Đ$[b]	# of short chain branches per 100 backbone carbons[c]
hPB-06	97	1.01	1.5
hPB-33	57	1.02	9.9
hPB-60	111	1.02	21.4
hPB-61	130	1.02	21.9
hPB-86	125	1.02	37.7
HDPE	50	2.08	0
PEP	120	1.03	25.5
PCHE	200	1.04	50
CEC[d]	30 (35)[e]	1.02 (1.02)[e]	C: 50; E: 2.4 (2.2)[e]

[a]hPBs listed as "hPB-x", where x = % 1,2-addition in PB. Other polymer abbreviations are defined in the main text. [b]M_n and dispersity $Đ = M_w/M_n$ values for hPB determined from SEC with multi-angle light scattering and reported dn/dc values in 1,2,4-trichlorobenzene at 135 °C,[87] whereas values for PEP, PCHE, and CEC, relied on a 100% mass recovery assumption in the SEC analyses. Values for HDPE provided based on Mark−Houwink analysis.[88,89] [c]Determined by ^{1}H NMR of the polydiene precursor. [d]62 wt % C and 38 wt % E based on ^{1}H NMR analysis. [e]Parenthetical values provided from Dow Chemical Co. as reported previously.[77]

Temperature-Dependent Degradation of hPB-60. We first probed the impact of temperature (T) on hydrogenolysis catalyzed by Pt−Re/SiO_2 by performing degradation experiments with hPB-60 at T = 140, 170, and 200 °C under 500 psig $H_2(g)$ for 17 h. To characterize the reaction products, SEC data plotted as intensity versus elution time (Figure S27) was recast as intensity versus number-average molecular weight (M_n) using the Mark−Houwink correlation for short-chain branched polyolefins in TCB at 135 °C,[90] as shown in Figure 3. A detailed description of this conversion and molecular weight correction by ethyl branch content is provided in the SI. By virtue of the near constant value of the refractive index increment dn/dc for the hPB-60 starting material and its degradation products, the intensity as a proxy for the relative mass fractions of chains of a given molar mass. These results revealed that the hydrogenolysis outcome over Pt−Re/SiO_2 strongly depends on temperature, such that hPB-60 is largely unreacted at 140 °C, yet it is degraded to a peak molar mass

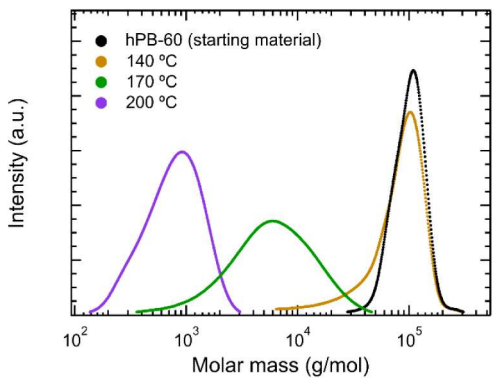

Figure 3. Polymer precursor SEC data for hPB-60 and products of its temperature-dependent hydrogenolytic degradation in cyclohexane over pretreated Pt−Re/SiO_2 (1:1 w/w polymer:catalyst) after 17 h at 140 °C (*orange*), 170 °C (*green*), and 200 °C (*purple*). M_n and $Đ$ values are provided in Table S6 as calculated using a Mark−Houwink correlation (see Experimental Methods for details).

M_{peak} < 1000 g/mol at 200 °C; note that the lowest M_n fragments approach the exclusion limit of the SEC instrument in the latter case. At 170 °C, an intermediate extent of degradation occurred. Consequently, we selected this condition to explore the role of polymer short-chain branching on the hydrogenolytic degradation kinetics. To further characterize the polymer degradation products, [−CH_2−]:[−CH_3] peak ratios were calculated from quantitative ^{1}H NMR spectra and their T_g values were extracted from DSC measurements for comparison to those obtained from the hPB-60 starting material (Table S6). The relative methyl peak intensity increased upon degradation (Figure S28), consistent with a greater number of end groups as expected for lower M_n products, and T_g monotonically decreased (Figure S29) concordant with the expected dependence of T_g on molecular weight.[91]

Polymer Hydrogenolysis Kinetics. Hydrogenolysis was carried out on HDPE, hPB-06, hPB-33, hPB-61, and hPB-86 at 170 °C and for selected cases small aliquots (ca. ≈ 20 mL) were sampled from the reactor at 1, 3, 5.75, and 7.75 h during each 17 h reaction. The resulting molecular weight distributions are presented in Figure 4, where SEC results were converted from retention time to molecular weight from Figure S30 or S32 as described above. Reaction replicates were performed to establish reproducibility of the results (Figures S31−S33 and Tables S10−S12). These data demonstrate that all of the initial polymer chains, except hPB-86, are consumed during the course of the reactions and yield either $M_n \cong 1000$ g/mol for HDPE, hPB-06 and hPB-33, or $M_n \cong 3000$ g/mol for hPB-61 after 17 h. Notably, hPB-86 exhibits almost no change in molecular weight over the course of the hydrogenolysis reaction.

For reactions of hPB-06, hPB-33, and hPB-61 that results in appreciable chain degradation, early time reaction aliquots exhibit bimodal molar mass distributions comprising combinations of unreacted and narrow dispersity starting material and broad distributions of cleaved chains with $M_{n,peak}$ = 10 000−20 000 g/mol (see Figures S34 and S35 for a description of the deconvolution of the overlapping SEC peaks in these data). This observation crucially implies that adsorption of an unreacted polymer molecule to the heterogeneous catalyst surface is followed by multiple hydrogenolysis reactions prior to surface desorption, reminiscent of a hydrogenation mechanism previously reported by Rosedale and Bates.[92] Subsequently, readsorption of the fragmented polymers followed by additional chain cleavage events drives the overall molar mass distribution to a monomodal form centered at the aforementioned lower M_n values.

Here we note that rudimentary calculations of the time required for the polymer coils to diffuse into the catalyst pores from the well-mixed, relatively dilute, solution (seconds) is much shorter than the reaction time associated with the bimodal molecular weight distributions, ruling out mass transfer limitations as the cause of these early time reaction outcomes. (A host of additional factors will influence the overall reaction kinetics including catalyst pore confinement effects, solvent quality, and competition between the solvent and polymer for surface adsorption. Our experiments have been designed to minimize the consequences of these effects, e.g., use of an ultrawide-pore catalyst and a good nonpolar solvent, in determining the relative impact of chain branching in polyolefin hydrogenolysis). Overall, hPB-06 reacts more

https://doi.org/10.1021/acscatal.5c04494
ACS Catal. 2025, 15, 16924−16937

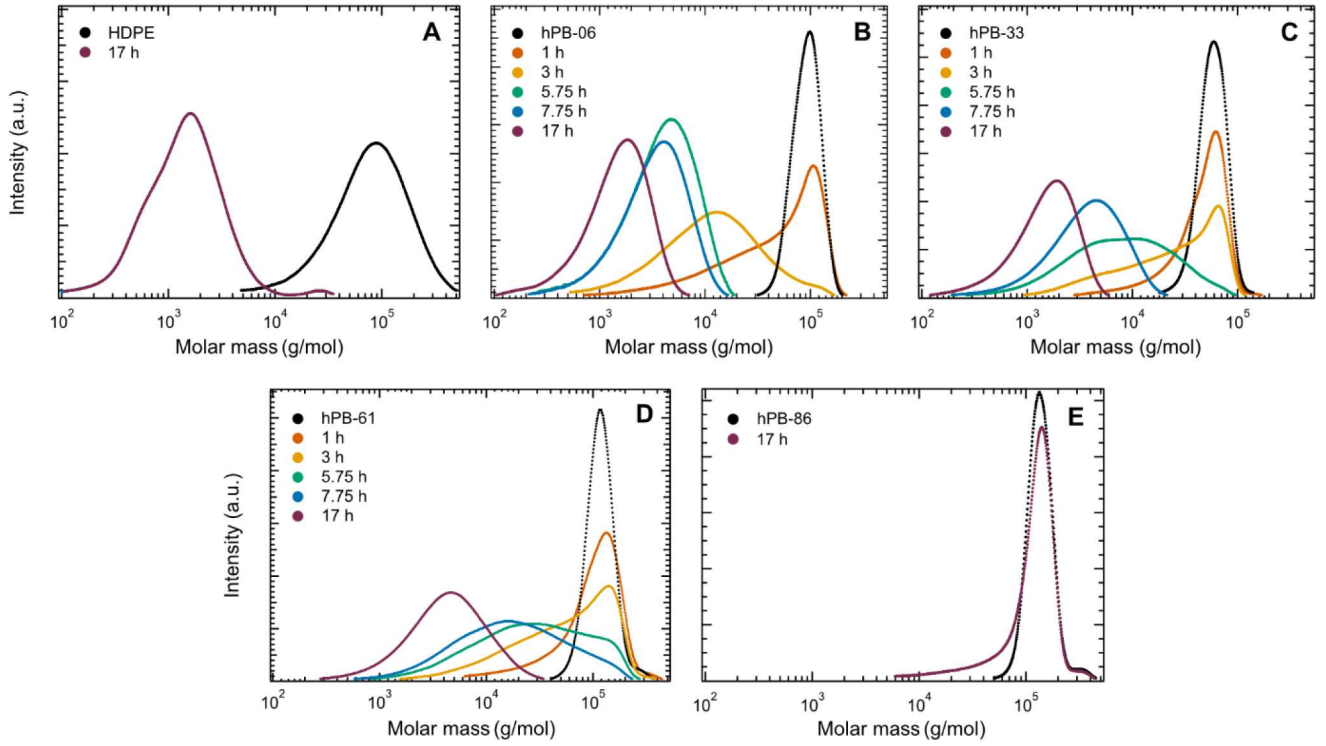

Figure 4. Molecular weight distributions of the initial model polyolefins (*black*) and reaction time-dependent degradation products arising from catalytic hydrogenolysis reactions at 170 °C with 1.0 g polymer and 1.0 g pretreated Pt−Re/SiO_2 in 130 mL cyclohexane under static 500 psig H_2(*g*): (A) HDPE, (B) hPB-06, (C) hPB-33, (D) hPB-61, and (E) hPB-86.

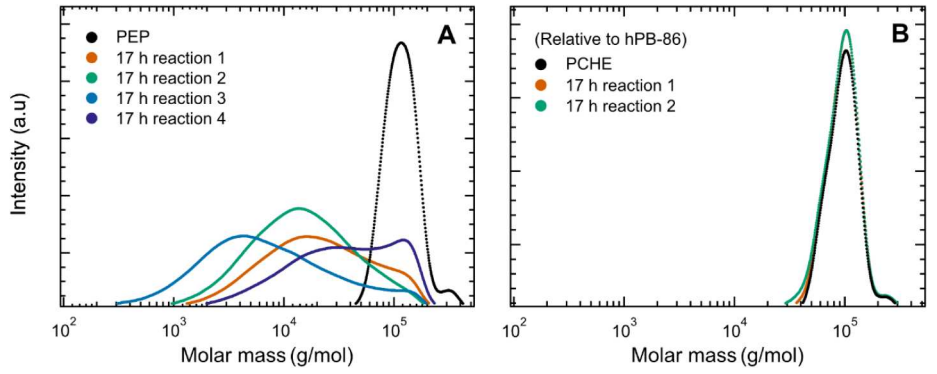

Figure 5. Intensity versus molecular weight plots from hydrogenolysis reaction replicates for (A) PEP and (B) PCHE in 17 h reactions at 170 °C with 1.0 g polymer and 1.0 g pretreated Pt−Re/SiO_2 in 130 mL cyclohexane. Molecular weight distributions for unreacted and reacted PCHE are presented using the Mark−Houwink parameters for hPB-86, as exact values are not available for PCHE.

quickly than hPB-33, which reacts faster than hPB-61, suggesting that the rate of polymer hydrogenolysis depends on the degree of short chain branching in the polymeric starting material. Again, the degraded polymers exhibit expected changes in their ^{1}H NMR spectra (Figure S36), T_g's, and their melting temperatures T_m (Figure S37) as summarized in Tables S7−S9.

Hydrogenolysis of PEP and PCHE. In order to assess the influence of side chain chemical structure and density along the all carbon backbone, hydrogenolysis reactions with Pt−Re/SiO_2 were conducted on PEP and PCHE at 170 °C for 17 h. Figures 5A (and Table S11, Figure S38A) shows the results for PEP, which exhibits a pendant methyl group on every fourth carbon atom, along with a statistical distribution of 1.5 isopropyl groups per 100 backbone carbon atoms. On average, chain cleavage in PEP is less extensive than with hPB-61, which displays a similar density of side chains (22 ethyl branches per 100 backbone carbon atoms); $\langle M_n\rangle_{PEP} \cong$ 9000 g/mol and $\langle M_n\rangle_{hPB\text{-}61} \cong$ 3000 g/mol. This disparate reactivity is also evident after 17 h at 200 °C, where PEP and hPB-60 are reduced to 1,100 and 600 g/mol, respectively (Figure S39). Also, the results shown in Figure 5A include noticeable fractions of unreacted polymer, not present in any of the hPB-61 reaction products. We return to this observation in the Discussion section. Additionally, the variability in the degraded product M_n-values across 4 PEP replicates is greater than that obtained with 3 replicates from hPB-61 (Figure S31D); we do not believe this is statistically significant given the limited number of experiments.

PCHE reacts strikingly differently from all of the other polymers in hydrogenolysis over the Pt−Re/SiO_2 catalyst, with the exception of hPB-86. After 17 h at 170 °C, there is virtually

https://doi.org/10.1021/acscatal.5c04494
ACS Catal. 2025, 15, 16924−16937

no decrease in M_n of the reaction product as illustrated in Figure 5B. However, ^{1}H NMR revealed the appearance of an additional peak at δ 0.9 ppm following the exposure to the catalyst under these reaction conditions (Figure S40), indicative of the formation of additional methyl groups. Inverse-gated decoupled ^{13}C NMR spectra obtained in 90/10 v/v 1,2-dichlorobenzene/1,1,2,2-tetrachloroethane-d_2 with chromium(III) acetylacetonate as a spin−lattice (T_1) relaxation agent[82] demonstrate the emergence of two weak resonances at δ 13.4 and 15.0 ppm after the catalytic reaction, which we associate with the ring opening of ∼1 mol % of the pendant cyclohexyl moieties in PCHE (Figure S41). As a control experiment to assess the degree and extent of cyclohexane solvent ring-opening, pure cyclohexane was subjected to the hydrogenolysis conditions for 17 h at 170 °C and static 500 psig $H_2(g)$ with the same catalyst loading. ^{1}H NMR and tandem gas chromatography−mass spectrometry analyses of the products revealed that 0.3 mol % and <1 mol % of the solvent had ring-opened to *n*-hexane, respectively; the explicit experimental protocols and results are described in the Supporting Information, and the results are summarized in Figures S42 and S43. Data from gas chromatography with flame-ionization detection (shown in Figure S43) corroborate these results.

DISCUSSION

Role of Branching in Hydrogenolysis. A compilation of the results of hydrogenolytic degradation experiments of eight differently branched model saturated hydrocarbon polymers at 170 °C provides previously unrecognized insights into the impact of branch content and structure on polymer degradation. Polymer hydrogenolysis is apparently hindered by sterically bulky side chains, which likely prevent backbone adsorption to the catalyst for subsequent chain cleavage. On the other hand, less branched polymers can adsorb sequences of backbone methylene units onto active metal sites for C−C bond scission and addition of hydrogen to yield lower M_n products. Figure 6 summarizes the time-dependent evolution of the reaction product molecular weight and distribution associated with all the hydrogenolysis reactions conducted at 170 °C, as well as the fractional reduction in molecular weight after t = 17 h at 170 °C, defined as

$$\text{Fractional reduction} = 1 - \frac{(M_n(t = 0\,\text{h}) - M_n(t = 17\,\text{h}))}{M_n(t = 0\,\text{h})} \quad (1)$$

The final molecular weights $M_n(t$ = 17 h) observed during hydrogenolysis of hPB-x and HDPE (i.e., hPB-0), exhibit the trend HDPE ≈ hPB-06 < hPB-33 < hPB-61 ≪ hPB-86. We note that similar conclusions can be drawn by considering the fractional reduction in molecular weight, albeit hPB-33 degrades more similarly to hPB-61 when assessed by this metric because its initial molecular weight $M_n(t = 0\,\text{h})$ is lower.

For hPB-0 and hPB-06, polymers with short-chain branch contents of either 0 or 1.5 ethyl branches/100 backbone carbons respectively, the final M_n and $Đ$ (see Table S10) of degradation products are similar. Thus, low concentrations of ethyl branches minimally impact the overall reaction rate and outcomes. From these findings, we conclude that tertiary carbon centers do not apparently drive the hydrogenolysis reaction. Furthermore, isolated ethyl branches along the all-carbon backbone do not appreciably affect polymer adsorption on the heterogeneous catalyst surface.

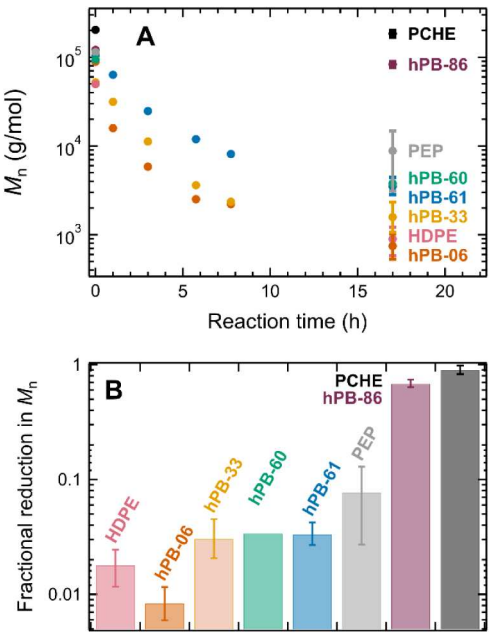

Figure 6. (A) M_n as a function of reaction time determined from the results shown in Figures 3-5 and S31. All data represent the mean $\langle M_n \rangle$ for y reaction replicates, with error bars representing the data range for HDPE, hPB-06, hPB-33, and hPB-61 (all with y = 3), PEP (y = 4), PCHE and hPB-86 (y = 2), and hPB-60 (y = 1). For times 1 ≤ t ≤ 7.75 h, reported values reflect single measurements (y = 1). (B) Fractional reduction in molecular weight for the specimens per (eq 1) with corresponding error bars from panel A. All molecular weights are from a Mark−Houwink analysis except for PCHE, which uses 100% mass recovery.

Presumably, runs of backbone methylene units present the active metal sites on the Pt−Re particles with pairs of cleavable backbone carbon atoms as illustrated in Figure 7. Random

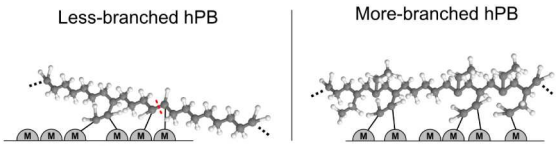

Figure 7. Illustration of the adsorption of less-branched hPB (*left*) or more-branched hPB (*right*) to a portion of the metal nanoparticle surface.[93] The presence of ethyl branches sterically hinders methylene adsorption and subsequent polymer backbone activation, effectively preventing chain cleavage.

chain cleavage is anticipated to lead to a most-probable molecular weight distribution, i.e., $Đ \rightarrow 2$, after numerous hydrogenolysis reactions, but prior to the limit of complete reaction, i.e., formation of methane.[91] Conversely, the higher ethyl branch contents in hPB-61 and hPB-86 sterically encumber the backbone and prevent its presentation to the catalyst surface for C−C bond activation (Figure 7), slowing (hPB-61) and ultimately extinguishing (hPB-86) the rate of degradation. This behavior parallels previous work on H/D exchange with hPBs on Pt−Re/SiO_2, where hydrogen−deuterium exchange by C−H bond activation occurs preferentially on the pendant ethyl groups versus backbone methylene moieties,[70] and occurs much more readily with

https://doi.org/10.1021/acscatal.5c04494
ACS Catal. 2025, 15, 16924−16937

HDPE relative to *i*PP.[71] However, a direct comparison of the previously reported H/D exchange behavior with the hydrogenolysis reactivity disclosed here is not entirely possible, due to differences in catalyst pretreatment prior to reaction (*vide infra*).

To assess the microstructural differences between the last two polymers that exhibit limited reactivities, quantitative ^{13}C NMR spectra were acquired for hPB-61 and hPB-86 (Figure S44). Integration of ^{13}C resonances associated with monomer sequence triads corresponding to backbone methylene units at 30.0 ppm indicate that they are present in lower concentrations in hPB-86 relative to hPB-61, in accordance with the expected statistical distributions of 1,2- and 1,4-butadiene additions in the anionic polymerizations used to produce the model polyolefins for this study.[94] The ^{13}C NMR spectrum of a hydrogenolyzed hPB-61 specimen indicates little change as compared to that of pristine hPB-61 (Figure S45); the ∼30 chain cleavage events per reacted macromolecule represent <0.4% of the carbon atoms in the polymer chain, hence significant change in the spectrum after hydrogenolysis is not expected. However, the degraded hPB-61 exhibits five new, small peaks in the chemical shift range δ 14−25 ppm arising from additional methyl end groups in the degraded, low molecular weight products. The associated stoichiometry is consistent with the reduction in molecular weight deduced by SEC, confirming limited participation of tertiary carbon sites in the hydrogenolysis reactions.

Two discrete populations of polymer molecular weights are clearly observed during the initial stages of hPB-06, hPB-33, and hPB-61 hydrogenolysis reactions (Figures 4 and S30), which offers insight into the reaction mechanism leading to depletion of the starting material. Peak molecular weights between 10 and 20 kg/mol for the degraded chains at early times indicate the initial polymer molecules are cleaved 5 to 10 times on average following adsorption on the surface of the catalyst and desorption of the fragments. This observation concurs with findings by molecular dynamics simulations by Vlachos and coworkers demonstrating that long-chain PE outcompetes short-chain PE in adsorption on a Pt(111) surface.[36,95,96] Apparently, multiple bond breaking occurs after this initial macromolecular adsorption step and prior to desorption. At a critical extent of reaction, the resulting low molecular weight polymer (M_{crit}) is displaced by unreacted high-M_n chains (Figure S46), presumably driven by a combination of their lower entropy of dissolution (scales as $1/M_n$) and the stronger multidentate binding of the longer chains to the catalyst.[91] Once the initial (unreacted) polymer is consumed, further chain cleavage events continually drive down the reaction product M_n. We further postulate that sections of the polymer are dynamically presented to the catalyst surface while bound through dehydrogenation and rehydrogenation events, as documented by Zhao et al. using magic-angle spinning NMR during an *in situ* hydrogenolysis of PE over a Pt/SiO_2 catalyst with a mesoporous silica shell (albeit in the absence of any solvent).[97] Such a dynamic macromolecule-catalyst binding mechanism is also consistent with H/D exchange in PE catalyzed by this $Pt–Re/SiO_2$ documented in earlier publications.[71,72]

Interestingly, PEP hydrogenolysis is somewhat slower than degradation of hPB-61 in spite of comparable short-chain branch densities: 25 methyl and 22 ethyl branches per 100 backbone carbons, respectively. This difference is exemplified by the presence of 3−24 wt % unreacted PEP chains across four replicates in 17 h reactions, as compared to 13 wt % unreacted hPB-61 chains after only 5.75 h of reaction (Figure S47). Based on ^{13}C NMR characterization of hPB-61, tertiary carbon atoms are separated by runs of either 1 or 5 $-CH_2-$ groups (with a small fraction of 9 or more methylenes in a row) along the backbone due to the statistical distribution of 1,4 and 1,2 repeat units in the polydiene precursor PB-61. On the other hand, PEP is characterized by precisely 3 methylene groups between tertiary carbons bearing a methyl side group (neglecting the minor fraction of isopropyl side chains arising from 5% 3,4-addition of isoprene in the otherwise 1,4-polyisoprene precursor). We assert that the occurrence of longer sequences of methylene groups in hPB-61 affords greater opportunities for local coordination of $-CH_2-CH_2-$ units with active sites on the catalyst resulting in a faster overall reaction rate, even though PEP has essentially the same number of backbone methylene groups per 100 backbone carbon atoms. Squeezing out virtually all sequences of methylene groups as in hPB-86 nearly extinguishes hydrogenolysis at 170 °C over 17 h, consistent with this hypothesis.

The resistance to hydrogenolysis exhibited by PCHE agrees well with the above trends and mechanistic deductions derived from the different reactivities of the hPBs and PEP materials. Along with a complete absence of methylene sequences, *syn*-pentane interactions between the bulky cyclohexyl rings on every other backbone carbon inhibit the formation of the chain extended *trans* backbone conformations implicated in PE hydrogenolysis (Figure 7).[36,98] The stability of this polymer under the conditions used to saturate PS is consistent with the original motivation behind development of the $Pt–Re/SiO_2$ catalyst for commercial use. Moreover, as we have shown, the pendant cyclohexyl groups are resistant to ring opening, which would detract from the useful physical properties of the resulting PCHE plastic (e.g., elevated T_g). We note that the commercial hydrogenation of PS employs much lower catalyst loadings than used in this work, which renders the possible hydrogenolysis of the cyclohexane group even less significant.

Overall, our experiments and interpretations shed fresh light on the reaction of polyolefins on heterogeneous catalysts. Figure 8 summarizes a striking correlation between the number of methylene groups between tertiary carbon atoms in the backbone and the final molecular weight obtained after a 17 h hydrogenolysis reaction over the $Pt–Re/SiO_2$ catalyst at 170 °C. Although we have restricted our attention to dilute

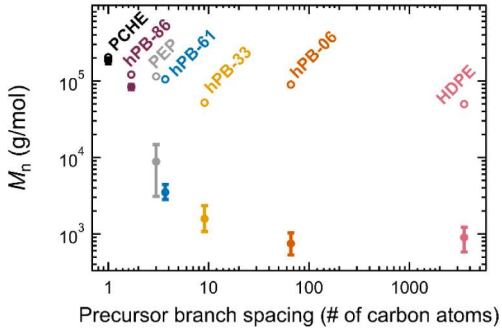

Figure 8. M_n of the model polyolefin starting materials (*open circles*) and their products from catalytic hydrogenolysis for 17 h over the $Pt–Re/SiO_2$ catalyst at 170 °C (*filled circles*) as functions of the average number of methylene groups between tertiary backbone carbons (summarized in Table S13). Error bars denote the observed data range.

https://doi.org/10.1021/acscatal.5c04494
ACS Catal. 2025, 15, 16924−16937

polymer solutions in cyclohexane, we believe the conclusions of this work regarding the role of branching are likely relevant to upcycling hydrocarbon polymers in the melt state.[8,9] Future work will be directed at increasing the polyolefin concentration up to the undiluted melt state, which will require dramatically different reactor designs (e.g., twin screw extrusion) and experimental protocols. Moreover, a host of additional factors will impact the ability of undiluted polymers to be upcycled, including high viscosity associated with entanglements, which restricts pore diffusion, heat transfer limitations, and possibly restricted configurational states on the catalyst surface.

Hydrogenolysis of Commercial CEC. While studies have thus far focused on the hydrogenolysis of model LLDPE materials with specific branch contents, realistic single-use plastic waste streams are inevitably mixtures of polyolefins with variable structures and short chain branch contents. However, assessing the reactivities of mixtures of the hPB polymers to address this issue is hampered by the fact that the SEC analyses do not readily provide access to the chemical constitution of the chromatographically separated species. In an initial attempt to overcome this problem, we considered an internal competition hydrogenolysis experiment using a CEC triblock polymer (see Figure 1), comprising an E block with 2.4 ethyl branches per 100 backbone C atoms (from ^{1}H NMR) akin to hPB-06 that is flanked by two PCHE end segments. We note that this CEC polymer is commercially produced by saturation of PS−PB-PS triblock using the Pt−Re/SiO_2 catalyst under conditions similar to those reported here, although at much lower catalyst loadings without catalyst pre-treatment.

Reaction of a 1 wt % cyclohexane solution of this CEC block polymer at 170 °C under 500 psig $H_2(g)$ for 17 h using a 1:1 *w*/*w* polymer to catalyst loading resulted in the chain degradation documented by the SEC data presented in Figure 9. The dispersity of the cleaved, lower M_n product is

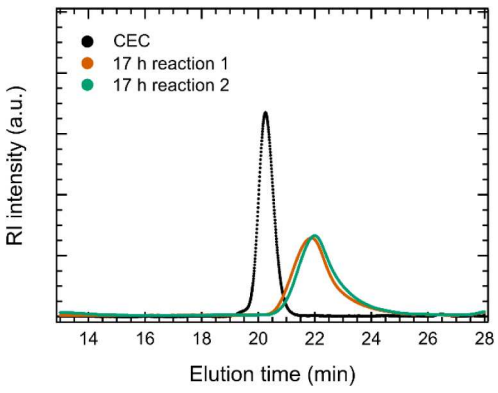

Figure 9. High temperature SEC data obtained in TCB at 135 °C for the initial CEC triblock (*black*) and the products of two replicate hydrogenolysis reactions over the pretreated Pt−Re/SiO_2 catalyst at 170 °C (*orange* and *green*).

considerably greater than that of the starting CEC ($Đ$ = 1.3 versus $Đ \cong 1.02$, respectively) yet not as high as that encountered with the model polyolefins.

Understanding the reaction course for CEC on Pt−Re/SiO_2 requires accounting for the different behaviors of the C versus E blocks in contact with the bimetallic catalyst and in solution. The SEC data in Figure 9 provide illuminating clues as to the mechanism of triblock copolymer degradation. The molecular weight distribution after reaction ($Đ \cong 1.3$) is consistent with the formation of CE diblocks by E segment cleavage, wherein the broader $Đ$ stems from convolution of narrow dispersity C chains ($Đ \cong 1.02$) connected to a disperse array of E chains (approaching $Đ \cong 2$ as discussed above) weighted according to the chain composition. We associate the low molecular weight tail on the SEC trace of the degraded material with the presence of a small number of E chains cleaved from the CE diblocks, which form in the initial stages of the hydrogenolysis reaction. Complete decoupling of the C blocks by E midblock cleavage accords with expectations based on the complete digestion of pristine HDPE, hPB-06, hPB-33, and hPB-61 after 17 h (Figure 4). Note that if the E blocks were completely consumed, we would expect to see a sharp peak in the SEC trace due to the remaining narrow dispersity C chains, along with a broad peak associated with the E oligomers, neither of which are evident. As discussed below, catalyst pretreatment increases its reactivity. Untreated Pt−Re/SiO_2 catalyst leads to a higher-M_n CE diblock product with fewer E fragments (Figure S48). This reinforces our proposed mechanism of rapid chain adsorption and E midblock cleavage, followed by slower hydrogenolysis of the E end blocks, mirroring the behavior documented with the homopolymers. This discrimination of reaction rates between the two stages of CEC degradation is likely amplified by the different propensities for C and E adsorption onto the metal catalyst, and the reduction in molecular weight after the initial bond cleavage that enhances dissolution of the CE diblock copolymer in cyclohexane versus binding to the catalyst surface.

Catalyst Pretreatment. As outlined in the Experimental section, all catalytic reactions were conducted with Pt−Re/SiO_2, pretreated by vacuum drying overnight at 100 °C. This conditioning step was motivated in part by a vinegar-like smell associated with the bulk catalyst. Dried and undried catalyst samples (100 mg) were stirred in THF-d_8 for ∼2 h and the resulting solutions were analyzed by ^{1}H NMR. Figure S49 reveals the presence of acetic acid,[99] which was largely removed by the vacuum treatment, evidenced by a ∼90% decrease in the peak intensity for acetic acid relative to the residual protiated solvent peak in THF-d_8 at δ 3.6 ppm. Hydrogenolysis reactions conducted with both forms of the catalyst revealed considerable differences in time-dependent hydrogenolysis outcomes as summarized in Figures S50 and S51. Reaction of hPB-60 for 17 h over the untreated catalyst resulted in significant variability in the distribution of product molecular weights between repeat experiments, including the presence of a significant amount of unreacted polymer (16 and 37 wt % in two replicate reactions). Conversely, when subjected to an identical procedure, but using the vacuum treated catalyst, hPB-60 was degraded to roughly a 5-fold lower average molar mass (Figure S50). Moreover, as noted previously, the extent of hydrogenolysis of CEC was enhanced by pretreating the catalyst as illustrated in Figure S48.

These results aid in resolving puzzling differences in the hydrogenolysis results reported by Ertem et al. versus what we have presented here.[75] That earlier study, also associated with deuterium exchange on various saturated hydrocarbon polymers, found limited degradation of HDPE and PEP under the same conditions reported here, albeit in isooctane instead of cyclohexane, in sharp contrast with the results shown in Figures 4A and 5A, respectively. However, we now believe that this can be attributed to the use of the untreated and thus less reactive Pt−Re/SiO_2 catalyst. Another curious finding in the earlier work was extensive degradation of a linear

https://doi.org/10.1021/acscatal.5c04494
ACS Catal. 2025, 15, 16924−16937

low-density PE (Exxon Exceed 1018 LLDPE), which appeared to implicate side chain branching in the mechanism of hydrogenolysis, contrary to what we have concluded presently. Exceed 1018 is a copolymer of ethylene and 1-hexene with about 1.3 butyl side chains per 100 backbone carbon atoms as opposed to 1.5 ethyl side chains per 100 backbone carbons in hPB-06. This outcome seems inconsistent with the less reactive untreated catalyst and may reflect a genuine effect associated with butyl branch adsorption onto or C−H activation by the metal surface followed by tertiary carbon bond cleavage possibly through a transient five-membered metallacyclic intermediate. Such reactions could lead to linear $\langle M_n \rangle \approx 10^3$ g/mol PE without involving the bond cleavage mechanism associated with the polyolefins presented in this work. Resolving this issue will require additional experiments with the vacuum-treated catalyst.

CONCLUSION

Hydrogenolysis of polyolefins dissolved in cyclohexane sensitively depends on the degree of short-chain branching. Using a small library of model polyethylenes with $M_n \sim 10^5$ g/mol bearing ethyl (hPB), methyl (PEP), cyclohexyl (PCHE), or no (HDPE) side chains produced by anionic polymerization or ring-opening metathesis polymerization and tandem hydrogenation, a correlation between branch content and temperature-dependent susceptibility to hydrogenolysis over a macroporous Pt−Re/SiO_2 catalyst was discovered. Using hPB-60 with 21 ethyl branches per 100 backbone carbons, we found that the hydrogenolysis reaction strongly depends on temperature, with almost no degradation at 140 °C, a modest extent of chain scission at 170 °C, and rapid hydrogenolysis at 200 °C, over a 17 h period. Time-dependent experiments at 170 °C revealed multiple chain cleavage events following initial adsorption onto the catalyst for polymers with 1.5−22 branches per 100 backbone carbon atoms. Little reaction occurred with 38 ethyl side chains per 100 backbone atoms, and there was no observed change in the molecular weight with PCHE. A commercial triblock copolymer CEC, containing hydrogenated polystyrene (C) end blocks coupled through a saturated polybutadiene (E, with 2.2 ethyl branches per 100 backbone atoms), exhibited partial cleavage of the E blocks and no degradation of the C blocks reflecting mixed susceptibility of this hybrid chain microstructure. These findings will aid in developing plastic waste upcycling strategies for converting saturated hydrocarbon polymers and their mixtures into commercially useful low molecular weight products.

ASSOCIATED CONTENT

Supporting Information

The Supporting Information is available free of charge at https://pubs.acs.org/doi/10.1021/acscatal.5c04494.

Reactor setup, reagent amounts for synthesis, HAADF-STEM line scans and EDX fitting, BET and XPS experimental details and results, NMR spectra of precursor polyolefins and select degraded products, SEC calculation details and chromatograms of precursor polyolefins and select degraded products, DSC traces of precursor polyolefins and select degraded products, raw SEC chromatograms of all degraded products, SEC molecular weight distributions and raw chromatograms of hydrogenolysis replicates, tables summarizing M_n, $Đ$, NMR peak intensities, and DSC thermal transitions for degradations, GC-MS and GC-FID data on ring-opened cyclohexane, ^{13}C NMR spectra of hPBs, NMR spectra of organic impurity in Pt−Re/SiO_2 catalyst, SEC chromatograms for untreated catalyst reactions, calculation of average branch spacing, experimental details and additional characterization data (PDF)

AUTHOR INFORMATION

Corresponding Authors

Mahesh K. Mahanthappa − *Department of Chemical Engineering and Materials Science, University of Minnesota, Minneapolis, Minnesota 55455, United States;* orcid.org/0000-0002-9871-804X; Email: maheshkm@umn.edu

Frank S. Bates − *Department of Chemical Engineering and Materials Science, University of Minnesota, Minneapolis, Minnesota 55455, United States;* orcid.org/0000-0003-3977-1278; Email: bates001@umn.edu

Authors

Zachary M. Gdowski − *Department of Chemical Engineering and Materials Science, University of Minnesota, Minneapolis, Minnesota 55455, United States*

Rishi Raj − *Department of Chemical Engineering and Materials Science, University of Minnesota, Minneapolis, Minnesota 55455, United States*

Aditya Bhan − *Department of Chemical Engineering and Materials Science, University of Minnesota, Minneapolis, Minnesota 55455, United States;* orcid.org/0000-0002-6069-7626

K. Andre Mkhoyan − *Department of Chemical Engineering and Materials Science, University of Minnesota, Minneapolis, Minnesota 55455, United States;* orcid.org/0000-0003-3568-5452

Complete contact information is available at: https://pubs.acs.org/10.1021/acscatal.5c04494

Notes

The authors declare no competing financial interest.

ACKNOWLEDGMENTS

Financial support for this work was provided by the American Chemical Society Petroleum Research Fund under grant 66786-ND7. ^1H NMR spectra used in this study were collected on a Bruker Avance III 500 MHz spectrometer, which is supported by the Office of the Director, National Institutes of Health, under Award Number S10OD011952. The content is solely the responsibility of the authors and does not necessarily represent the official views of the National Institutes of Health. The electron microscopy portion of this work was supported by NSF through award No. DMR-2309431, carried out in the Characterization Facility of the University of Minnesota, which receives partial support from the NSF through the MRSEC program under award DMR-2011401. We thank Matthew Jacob for acquisition of GC/FID, and Elijah Kipp and Bing Luo for BET and XPS measurements.

REFERENCES

(1) OECD *Global Plastics Outlook: economic Drivers, Environmental Impacts and Policy Options*; OECD Publishing: Paris, 2022. DOI: 10.1787/de747aef-en (last accessed 19 September 2025).

(2) Dokl, M.; Copot, A.; Krajnc, D.; Fan, Y. V.; Vujanović, A.; Aviso, K. B.; Tan, R. R.; Kravanja, Z.; Čuček, L. Global Projections of Plastic Use, End-of-Life Fate and Potential Changes in Consumption, Reduction, Recycling and Replacement with Bioplastics to 2050. *Sustainable Prod. Consumption* **2024**, *51*, 498−518.
(3) Borrelle, S. B.; Ringma, J.; Law, K. L.; Monnahan, C. C.; Lebreton, L.; McGivern, A.; Murphy, E.; Jambeck, J.; Leonard, G. H.; Hilleary, M. A.; Eriksen, M.; Possingham, H. P.; De Frond, H.; Gerber, L. R.; Polidoro, B.; Tahir, A.; Bernard, M.; Mallos, N.; Barnes, M.; Rochman, C. M. Predicted Growth in Plastic Waste Exceeds Efforts to Mitigate Plastic Pollution. *Science* **2020**, *369*, 1515−1518.
(4) Ryan, A. J.; Rothman, R. H. Engineering Chemistry to Meet COP26 Targets. *Nat. Rev. Chem.* **2022**, *6*, 1−3.
(5) Faust, K.; Denifl, P.; Hapke, M. Recent Advances in Catalytic Chemical Recycling of Polyolefins. *ChemCatchem* **2023**, *15*, No. e202300310.
(6) Goring, P. D.; Priestley, R. D. Polymer Recycling and Upcycling: Recent Developments toward a Circular Economy. *JACS Au* **2023**, *3*, 2609−2611.
(7) Korley, L. T. J.; Epps, T. H.; Helms, B. A.; Ryan, A. J. Toward Polymer Upcycling—Adding Value and Tackling Circularity. *Science* **2021**, *373*, 66−69.
(8) Xu, S.; Tang, J.; Fu, L. Catalytic Strategies for the Upcycling of Polyolefin Plastic Waste. *Langmuir* **2024**, *40*, 3984−4000.
(9) Ong, A.; Teo, J. Y. Q.; Lim, J. Y. C. Interfacial Reactions in Chemical Recycling and Upcycling of Plastics. *ACS Appl. Mater. Interfaces* **2024**, *16*, 46975−46987.
(10) Dufaud, V.; Basset, J.-M. Catalytic Hydrogenolysis at Low Temperature and Pressure of Polyethylene and Polypropylene to Diesels or Lower Alkanes by a Zirconium Hydride Supported on Silica-Alumina: A Step Toward Polyolefin Degradation by the Microscopic Reverse of Ziegler−Natta Polymerization. *Angew. Chem., Int. Ed.* **1998**, *37*, 806−810.
(11) Jia, C.; Xie, S.; Zhang, W.; Intan, N. N.; Sampath, J.; Pfaendtner, J.; Lin, H. Deconstruction of High-Density Polyethylene into Liquid Hydrocarbon Fuels and Lubricants by Hydrogenolysis over Ru Catalyst. *Chem. Catal.* **2021**, *1*, 437−455.
(12) Chen, L.; Zhu, Y.; Meyer, L. C.; Hale, L. V.; Le, T. T.; Karkamkar, A.; Lercher, J. A.; Gutiérrez, O. Y.; Szanyi, J. Effect of Reaction Conditions on the Hydrogenolysis of Polypropylene and Polyethylene into Gas and Liquid Alkanes. *React. Chem. Eng.* **2022**, *7*, 844−854.
(13) Borkar, S. S.; Helmer, R.; Panicker, S.; Shetty, M. Investigation into the Reaction Pathways and Catalyst Deactivation for Polyethylene Hydrogenolysis over Silica-Supported Cobalt Catalysts. *ACS Sustainable Chem. Eng.* **2023**, *11*, 10142−10157.
(14) Nakaji, Y.; Tamura, M.; Miyaoka, S.; Kumagai, S.; Tanji, M.; Nakagawa, Y.; Yoshioka, T.; Tomishige, K. Low-Temperature Catalytic Upgrading of Waste Polyolefinic Plastics into Liquid Fuels and Waxes. *Appl. Catal., B* **2021**, *285*, 119805.
(15) Kots, P. A.; Liu, S.; Vance, B. C.; Wang, C.; Sheehan, J. D.; Vlachos, D. G. Polypropylene Plastic Waste Conversion to Lubricants over Ru/TiO_2 Catalysts. *ACS Catal.* **2021**, *11*, 8104−8115.
(16) Jaydev, S. D.; Martín, A. J.; Pérez-Ramírez, J. Direct Conversion of Polypropylene into Liquid Hydrocarbons on Carbon-Supported Platinum Catalysts. *ChemSuschem* **2021**, *14*, 5179−5185.
(17) Lamb, J. V.; Lee, Y.-H.; Sun, J.; Byron, C.; Uppuluri, R.; Kennedy, R. M.; Meng, C.; Behera, R. K.; Wang, Y.-Y.; Qi, L.; Sadow, A. D.; Huang, W.; Ferrandon, M. S.; Scott, S. L.; Poeppelmeier, K. R.; Abu-Omar, M. M.; Delferro, M. Supported Platinum Nanoparticles Catalyzed Carbon−Carbon Bond Cleavage of Polyolefins: Role of the Oxide Support Acidity. *ACS Appl. Mater. Interfaces* **2024**, *16*, 11361−11376.
(18) Zhao, Z.; Li, Z.; Zhang, X.; Li, T.; Li, Y.; Chen, X.; Wang, K. Catalytic Hydrogenolysis of Plastic to Liquid Hydrocarbons over a Nickel-Based Catalyst. *Environ. Pollut.* **2022**, *313*, 120154.
(19) Kim, S.; Yang, B.; Gutiérrez, O. Y.; Zhang, W.; Lizandara-Pueyo, C.; Ingale, P.; Jevtovikj, I.; Grauke, R.; Szanyi, J.; Wang, H.; Schunk, S. A.; Lercher, J. A. Ru-Catalyzed Polyethylene Hydrogenolysis under Quasi-Supercritical Conditions. *JACS Au* **2025**, *5*, 1760−1770.
(20) Celik, G.; Kennedy, R. M.; Hackler, R. A.; Ferrandon, M.; Tennakoon, A.; Patnaik, S.; LaPointe, A. M.; Ammal, S. C.; Heyden, A.; Perras, F. A.; Pruski, M.; Scott, S. L.; Poeppelmeier, K. R.; Sadow, A. D.; Delferro, M. Upcycling Single-Use Polyethylene into High-Quality Liquid Products. *ACS Cent. Sci.* **2019**, *5*, 1795−1803.
(21) Chen, L.; Meyer, L. C.; Kovarik, L.; Meira, D.; Pereira-Hernandez, X. I.; Shi, H.; Khivantsev, K.; Gutiérrez, O. Y.; Szanyi, J. Disordered Sub-Nanometer Ru Structures on CeO_2 are Highly Efficient and Selective Catalysts in Polymer Upcycling by Hydrogenolysis. *ACS Catal.* **2022**, *12*, 4618−4627.
(22) Nguyen-Phu, H.; Kwon, T.; Kim, T.; Thi Do, L.; Hyuk Kang, K.; Ro, I. Investigating the Influence of Ru Structures and Supports on Hydrogenolysis of Polyethylene Plastic Waste. *Chem. Eng. J.* **2023**, *475*, 146076.
(23) Kang, Q.; Chu, M.; Xu, P.; Wang, X.; Wang, S.; Cao, M.; Ivasenko, O.; Sham, T.-K.; Zhang, Q.; Sun, Q.; et al. Entropy Confinement Promotes Hydrogenolysis Activity for Polyethylene Upcycling. *Angew. Chem., Int. Ed.* **2023**, *62*, No. e202313174.
(24) Tennakoon, A.; Wu, X.; Paterson, A. L.; Patnaik, S.; Pei, Y.; LaPointe, A. M.; Ammal, S. C.; Hackler, R. A.; Heyden, A.; Slowing, I. I.; Coates, G. W.; Delferro, M.; Peters, B.; Huang, W.; Sadow, A. D.; Perras, F. A. Catalytic Upcycling of High-Density Polyethylene Via a Processive Mechanism. *Nat. Catal.* **2020**, *3*, 893−901.
(25) Wu, X.; Tennakoon, A.; Yappert, R.; Esveld, M.; Ferrandon, M. S.; Hackler, R. A.; LaPointe, A. M.; Heyden, A.; Delferro, M.; Peters, B.; Sadow, A. D.; Huang, W. Size-Controlled Nanoparticles Embedded in a Mesoporous Architecture Leading to Efficient and Selective Hydrogenolysis of Polyolefins. *J. Am. Chem. Soc.* **2022**, *144*, 5323−5334.
(26) McCullough, K. E.; Peczak, I. L.; Kennedy, R. M.; Wang, Y.-Y.; Lin, J.; Wu, X.; Paterson, A. L.; Perras, F. A.; Hall, J.; Kropf, A. J.; Hackler, R. A.; Shin, Y.; Niklas, J.; Poluektov, O. G.; Wen, J.; Huang, W.; Sadow, A. D.; Poeppelmeier, K. R.; Delferro, M.; Ferrandon, M. S. Synthesis of Platinum Nanoparticles on Strontium Titanate Nanocuboids Via Surface Organometallic Grafting for the Catalytic Hydrogenolysis of Plastic Waste. *J. Mater. Chem. A* **2023**, *11*, 1216−1231.
(27) Peczak, I. L.; Kennedy, R. M.; Hackler, R. A.; Wang, R.; Shin, Y.; Delferro, M.; Poeppelmeier, K. R. Scalable Synthesis of $Pt/SrTiO_3$ Hydrogenolysis Catalysts in Pursuit of Manufacturing-Relevant Waste Plastic Solutions. *ACS Appl. Mater. Interfaces* **2021**, *13*, 58691−58700.
(28) Vance, B. C.; Kots, P. A.; Wang, C.; Granite, J. E.; Vlachos, D. G. Ni/SiO_2 Catalysts for Polyolefin Deconstruction Via the Divergent Hydrogenolysis Mechanism. *Appl. Catal., B* **2023**, *322*, 122138.
(29) Zhao, M.; Chu, X.; Wang, F.; Fang, Y.; Sun, L.; Xie, Q.; Zhang, L.-L.; Song, S.; Zhang, H.; Wang, X. Enhancing the Conversion Efficiency of Polyethylene to Methane through Codoping of Mn Atoms into Ru Centers and CeO_2 Supports. *J. Am. Chem. Soc.* **2024**, *146*, 33104−33111.
(30) Sun, J. A.; Kots, P. A.; Hinton, Z. R.; Marinkovic, N. S.; Ma, L.; Ehrlich, S. N.; Zheng, W.; Epps, T. H.; Korley, L. T. J.; Vlachos, D. G. Size and Structure Effects of Carbon-Supported Ruthenium Nanoparticles on Waste Polypropylene Hydrogenolysis Activity, Selectivity, and Product Microstructure. *ACS Catal.* **2024**, *14*, 3228−3240.
(31) Meirow, M.; Tennakoon, A.; Wu, X.; Willmon, J.; Howell, D.; Huang, W.; Sadow, A. D.; Luijten, E. Influence of Pore Length on Hydrogenolysis of Polyethylene within a Mesoporous Support Architecture. *J. Phys. Chem. C* **2023**, *127*, 23805−23813.
(32) Zhang, X.; Sun, B.; Zhao, Z.; Li, T.; Mate, M.; Wang, K. Polyethylene Hydrogenolysis over Bimetallic Catalyst with Suppression of Methane Formation. *Front. Chem. Sci. Eng.* **2024**, *18*, 110.
(33) Ji, H.; Wang, X.; Wei, X.; Peng, Y.; Zhang, S.; Song, S.; Zhang, H. Boosting Polyethylene Hydrogenolysis Performance of $Ru-CeO_2$ Catalysts by Finely Regulating the Ru Sizes. *Small* **2023**, *19*, No. e2300903.
(34) Wang, Y.-Y.; Tennakoon, A.; Wu, X.; Sahasrabudhe, C.; Qi, L.; Peters, B. G.; Sadow, A. D.; Huang, W. Catalytic Hydrogenolysis of

Polyethylene Under Reactive Separation. *ACS Catal.* **2024**, *14*, 2084−2094.
(35) Pennel, M. L.; Jiang, Y.; Cargnello, M. Influence of Autoclave Liner on Polyethylene Hydrogenolysis Selectivity. *ACS Sustainable Resour. Manage.* **2024**, *1*, 1047−1052.
(36) Zare, M.; Kots, P. A.; Caratzoulas, S.; Vlachos, D. G. Conformations of Polyolefins on Platinum Catalysts Control Product Distribution in Plastics Recycling. *Chem. Sci.* **2023**, *14*, 1966−1977.
(37) Hackler, R. A.; Lamb, J. V.; Peczak, I. L.; Kennedy, R. M.; Kanbur, U.; LaPointe, A. M.; Poeppelmeier, K. R.; Sadow, A. D.; Delferro, M. Effect of Macro- and Microstructures on Catalytic Hydrogenolysis of Polyolefins. *Macromolecules* **2022**, *55*, 6801−6810.
(38) Hackler, R. A.; Vyavhare, K.; Kennedy, R. M.; Celik, G.; Kanbur, U.; Griffin, P. J.; Sadow, A. D.; Zang, G.; Elgowainy, A.; Sun, P.; Poeppelmeier, K. R.; Erdemir, A.; Delferro, M. Synthetic Lubricants Derived from Plastic Waste and their Tribological Performance. *ChemSuschem* **2021**, *14*, 4181−4189.
(39) Rorrer, J. E.; Troyano-Valls, C.; Beckham, G. T.; Román-Leshkov, Y. Hydrogenolysis of Polypropylene and Mixed Polyolefin Plastic Waste over Ru/C to Produce Liquid Alkanes. *ACS Sustainable Chem. Eng.* **2021**, *9*, 11661−11666.
(40) Rorrer, J. E.; Beckham, G. T.; Román-Leshkov, Y. Conversion of Polyolefin Waste to Liquid Alkanes with Ru-Based Catalysts under Mild Conditions. *JACS Au* **2021**, *1*, 8−12.
(41) Ma, W.; Wang, C.; Chen, Z.; Yan, S.; Cao, S.; Wang, X.; Chen, Y.; Yang, H.; Chen, H. Catalytic Hydrogenolysis of Polypropylene and Polyethylene Mixtures: Effect of Temperature on Liquid Alkane Components. *J. Energy Inst.* **2024**, *115*, 101615.
(42) Zhang, F.; Zeng, M.; Yappert, R. D.; Sun, J.; Lee, Y.-H.; LaPointe, A. M.; Peters, B.; Abu-Omar, M. M.; Scott, S. L. Polyethylene Upcycling to Long-Chain Alkylaromatics by Tandem Hydrogenolysis/Aromatization. *Science* **2020**, *370*, 437−441.
(43) Balzer, A. H.; Hinton, Z. R.; Vance, B. C.; Vlachos, D. G.; Korley, L. T. J.; Epps, T. H. Tracking Chain Populations and Branching Structure during Polyethylene Deconstruction Processes. *ACS Cent. Sci.* **2024**, *10*, 1755−1764.
(44) Mason, A. H.; Motta, A.; Das, A.; Ma, Q.; Bedzyk, M. J.; Kratish, Y.; Marks, T. J. Rapid atom-efficient polyolefin plastics hydrogenolysis mediated by a well-defined single-site electrophilic/cationic organo-zirconium catalyst. *Nat. Commun.* **2022**, *13*, 7187.
(45) Mason, A. H.; Motta, A.; Kratish, Y.; Marks, T. J. Demystifying group-4 polyolefin hydrogenolysis catalysis: Gaseous propane hydrogenolysis mechanism over the same catalysts. *Proc. Natl. Acad. Sci. U. S. A.* **2024**, *121*, No. e2406133121.
(46) Edenfield, W. C.; Mason, A. H.; Lai, Q.; Agarwal, A.; Kobayashi, T.; Kratish, Y.; Marks, T. J. Rapid Polyolefin Plastic Hydrogenolysis Mediated by Single-Site Heterogeneous Electrophilic/Cationic Organo-group IV Catalysts. *ACS Catal.* **2024**, *14*, 554−565.
(47) Lai, Q.; Mason, A. H.; Agarwal, A.; Edenfield, W. C.; Zhang, X.; Kobayashi, T.; Kratish, Y.; Marks, T. J. Rapid Polyolefin Hydrogenolysis by a Single-Site Organo-Tantalum Catalyst on a Super-Acidic Support: Structure and Mechanism. *Angew. Chem., Int. Ed.* **2023**, *62*, e202312546.
(48) Gao, J.; Zhu, L.; Conley, M. P. Polypropylene Degradation Catalyzed by Tantalum Hydrides Supported on Sulfated Alumina. *ACS Catal.* **2023**, *13*, 10765−10769.
(49) Gao, J.; Zhu, L.; Conley, M. P. Cationic Tantalum Hydrides Catalyze Hydrogenolysis and Alkane Metathesis Reactions of Paraffins and Polyethylene. *J. Am. Chem. Soc.* **2023**, *145*, 4964−4968.
(50) Sinfelt, J. H. *Bimetallic Catalysts: discoveries, Concepts, and Applications*; Wiley, 1983.
(51) Falcone, D. D.; Hack, J. H.; Klyushin, A. Y.; Knop-Gericke, A.; Schlögl, R.; Davis, R. J. Evidence for the Bifunctional Nature of Pt−Re Catalysts for Selective Glycerol Hydrogenolysis. *ACS Catal.* **2015**, *5*, 5679−5695.
(52) Xiao, J.; Puddephatt, R. J. Pt-Re Clusters and Bimetallic Catalysts. *Coord. Chem. Rev.* **1995**, *143*, 457−500.
(53) Yu, W.; Porosoff, M. D.; Chen, J. G. Review of Pt-Based Bimetallic Catalysis: From Model Surfaces to Supported Catalysts. *Chem. Rev.* **2012**, *112*, 5780−5817.
(54) Kim, H. U.; Makolkin, N. V.; Kim, J.; Murali, V.; Jae, J. Controlled Synthesis of PtRe and NiRe Bimetallic Catalysts for Enhanced Biomass Hydrogenation. *Energy Fuels* **2024**, *38*, 16458−16472.
(55) Sinfelt, J. H. Heterogeneous Catalysis: Some Recent Developments. *Science* **1977**, *195*, 641−646.
(56) Sinfelt, J. H. Structure of bimetallic clusters. *Acc. Chem. Res.* **1987**, *20*, 134−139.
(57) Liu, L.; Corma, A. Bimetallic Sites for Catalysis: From Binuclear Metal Sites to Bimetallic Nanoclusters and Nanoparticles. *Chem. Rev.* **2023**, *123*, 4855−4933.
(58) Hucul, D. A.; Hahn, S. F. Catalytic Hydrogenation of Polystyrene. *Adv. Mater.* **2000**, *12*, 1855−1858.
(59) Bishop, J. P.; Register, R. A. Thermoplastic Elastomers with Composite Crystalline−Glassy Hard Domains and Single-Phase Melts. *Macromolecules* **2010**, *43*, 4954−4960.
(60) Myers, S. B.; Register, R. A. Crystallization of Defect-Free Polyethylene within Block Copolymer Mesophases. *Macromolecules* **2010**, *43*, 393−401.
(61) Burns, A. B.; Register, R. A. Mechanical Properties of Star Block Polymer Thermoplastic Elastomers with Glassy and Crystalline End Blocks. *Macromolecules* **2016**, *49*, 9521−9530.
(62) Burns, A. B.; Register, R. A. Thermoplastic Elastomers via Combined Crystallization and Vitrification from Homogeneous Melts. *Macromolecules* **2016**, *49*, 269−279.
(63) Bates, F. S.; Fredrickson, G. H.; Hucul, D.; Hahn, S. F. PCHE-Based Pentablock Copolymers: Evolution of a New Plastic. *AlChE J.* **2001**, *47*, 762−765.
(64) Calverley, E. M.; Patel, A.; Hucul, D. A.; Siddall, J. H. *Process for Hydrogenating Unsaturated Polymers*. US 6,395,841 B1, 2002.
(65) *ViviOn™ (CBC)- Cyclic Block Copolymers (CBCs)*; USI Corporation. https://www.usife.com/en-us/dirProduct/frmProduct6 accessed 16 June 2025.
(66) Cochran, E. W.; Bates, F. S. Thermodynamic Behavior of Poly(cyclohexylethylene) in Polyolefin Diblock Copolymers. *Macromolecules* **2002**, *35*, 7368−7374.
(67) Phatak, A.; Lim, L. S.; Reaves, C. K.; Bates, F. S. Toughness of Glassy−Semicrystalline Multiblock Copolymers. *Macromolecules* **2006**, *39*, 6221−6228.
(68) Mahanthappa, M. K.; Lim, L. S.; Hillmyer, M. A.; Bates, F. S. Control of Mechanical Behavior in Polyolefin Composites: Integration of Glassy, Rubbery, and Semicrystalline Components. *Macromolecules* **2007**, *40*, 1585−1593.
(69) Burns, A. B.; Register, R. A. Strategies for the Synthesis of Well-Defined Star Polymers by Anionic Polymerization with Chlorosilane Coupling and Preservation of the Star Architecture during Catalytic Hydrogenation. *Macromolecules* **2016**, *49*, 2063−2070.
(70) Zeng, Y.; López-Barrón, C. R.; Kang, S.; Eberle, A. P. R.; Lodge, T. P.; Bates, F. S. Effect of Branching and Molecular Weight on Heterogeneous Catalytic Deuterium Exchange in Polyolefins. *Macromolecules* **2017**, *50*, 6849−6860.
(71) Habersberger, B. M.; Lodge, T. P.; Bates, F. S. Solvent Selective Hydrogen−Deuterium Exchange on Saturated Polyolefins. *Macromolecules* **2012**, *45*, 7778−7782.
(72) Habersberger, B. M.; Hart, K. E.; Gillespie, D.; Huang, T. Molecular Weight Dependence of Deuterium Exchange on Polyethylene: Direct Measurement and SANS Model. *Macromolecules* **2015**, *48*, 5951−5958.
(73) Kang, S.; Zeng, Y.; Lodge, T. P.; Bates, F. S.; Brant, P.; López-Barrón, C. R. Impact of Molecular Weight and Comonomer Content on Catalytic Hydrogen-Deuterium Exchange in Polyolefins. *Polymer* **2016**, *102*, 99−105.
(74) López-Barrón, C. R.; Zeng, Y.; Schaefer, J. J.; Eberle, A. P. R.; Lodge, T. P.; Bates, F. S. Molecular Alignment in Polyethylene During Cold Drawing Using In-Situ SANS and Raman Spectroscopy. *Macromolecules* **2017**, *50*, 3627−3636.

(75) Ertem, S. P.; Onuoha, C. E.; Wang, H.; Hillmyer, M. A.; Reineke, T. M.; Lodge, T. P.; Bates, F. S. Hydrogenolysis of Linear Low-Density Polyethylene During Heterogeneous Catalytic Hydrogen−Deuterium Exchange. *Macromolecules* **2020**, *53*, 6043−6055.
(76) Pangborn, A. B.; Giardello, M. A.; Grubbs, R. H.; Rosen, R. K.; Timmers, F. J. Safe and Convenient Procedure for Solvent Purification. *Organometallics* **1996**, *15*, 1518−1520.
(77) Mori, Y.; Lim, L. S.; Bates, F. S. Consequences of Molecular Bridging in Lamellae-Forming Triblock/Pentablock Copolymer Blends. *Macromolecules* **2003**, *36*, 9879−9888.
(78) Gehlsen, M. D. *Catalytic Hydrogenation of Polymers: synthesis and Characterization of Model Polyolefins*. Ph.D. Dissertation, University of Minnesota, 1993.
(79) Gdowski, Z. M.; Swartzendruber, S. M.; Mahanthappa, M. K.; Bates, F. S. Diblock Copolymer Blends Do Not Mimic Metal Alloys. *Macromolecules* **2024**, *57*, 7926−7940.
(80) Sample, C. S.; Kellstedt, E. A.; Hillmyer, M. A. Tandem ROMP/Hydrogenation Approach to Hydroxy-Telechelic Linear Polyethylene. *ACS Macro Lett.* **2022**, *11*, 608−614.
(81) Jang, Y.-J.; Nguyen, S.; Hillmyer, M. A. Chemically Recyclable Linear and Branched Polyethylenes Synthesized from Stoichiometrically Self-Balanced Telechelic Polyethylenes. *J. Am. Chem. Soc.* **2024**, *146*, 4771−4782.
(82) Zhou, Z.; He, Y.; Qiu, X.; Redwine, D.; Potter, J.; Cong, R.; Miller, M. Optimum $Cr(acac)_3$ Concentration for NMR Quantitative Analysis of Polyolefins. *Macromol. Symp.* **2013**, *330*, 115−122.
(83) Kalinkin, A. V.; Smirnov, M. Y.; Nizovskii, A. I.; Bukhtiyarov, V. I. X-ray photoelectron spectra of platinum compounds excited with monochromatic AgLα irradiation. *J. Electron Spectrosc. Relat. Phenom.* **2010**, *177*, 15−18.
(84) Tysoe, W. T.; Zaera, F.; Somorjai, G. A. An XPS study of the oxidation and reduction of the rhenium-platinum system under atmospheric conditions. *Surf. Sci.* **1988**, *200*, 1−14.
(85) Gothe, M. L.; Silva, K. L. C.; Figueredo, A. L.; Fiorio, J. L.; Rozendo, J.; Manduca, B.; Simizu, V.; Freire, R. S.; Garcia, M. A. S.; Vidinha, P. A Rhenium Tuneable Player in Tailored Hydrogenation Catalysis. *Eur. J. Inorg. Chem.* **2021**, *2021*, 4043−4065.
(86) Young, R. N.; Quirk, R. P.; Fetters, L. J. Anionic Polymerizations of Non-Polar Monomers Involving Lithium. In *Anionic Polymerization*; Springer: Berlin Heidelberg, 1984; pp. 1−90.
(87) Sun, T.; Brant, P.; Chance, R. R.; Graessley, W. W. Effect of Short Chain Branching on the Coil Dimensions of Polyolefins in Dilute Solution. *Macromolecules* **2001**, *34*, 6812−6820.
(88) Wagner, H. L. The Mark−Houwink−Sakurada Equation for the Viscosity of Atactic Polystyrene. *J. Phys. Chem. Ref. Data* **1985**, *14*, 1101−1106.
(89) Wagner, H. L. The Mark−Houwink−Sakurada Equation for the Viscosity of Linear Polyethylene. *J. Phys. Chem. Ref. Data* **1985**, *14*, 611−617.
(90) Scholte, T. G.; Meijerink, N. L. J.; Schoffeleers, H. M.; Brands, A. M. G. Mark−Houwink Equation and GPC Calibration for Linear Short-Chain Branched Polyolefins, Including Polypropylene and Ethylene−Propylene Copolymers. *J. Appl. Polym. Sci.* **1984**, *29*, 3763−3782.
(91) Lodge, T. P.; Hiemenz, P. C. *Polymer Chemistry*; Taylor & Francis Group: Boca Raton, FL, 2020.
(92) Rosedale, J. H.; Bates, F. S. Heterogeneous Catalytic Hydrogenation of Poly(vinylethylene). *J. Am. Chem. Soc.* **1988**, *110*, 3542−3545.
(93) *DIY molecules*. https://biomodel.uah.es/en/DIY/JSME/draw.en.htm accessed 13 June 2025.
(94) Cheng, H. N. Carbon-13 NMR Characterization of Ethylene/1-Butene Copolymers. *Macromolecules* **1991**, *24*, 4813−4819.
(95) Zare, M.; Kots, P. A.; Hinton, Z. R.; Epps, T. H.; Korley, L. T. J.; Caratzoulas, S.; Vlachos, D. G. Effect of Reaction Media on Hydrogenolysis of Polyethylene Plastic Waste: Polymer-Surface Interactions in Small Alkane/Polymer Blends. *Appl. Catal., B* **2024**, *351*, 123969.
(96) Mehendale, R. M.; Vlachos, D. G.; Caratzoulas, S. Effect of Metal Catalyst Facets on Polyethylene Adsorption. *J. Phys. Chem. C* **2025**, *129*, 2000−2010.
(97) Zhao, T. Y.; Meirow, M.; Tennakoon, A.; Wu, X.; Paterson, A. L.; Qi, L.; LaPointe, A. M.; Lamb, J. V.; Kobayashi, T.; Delferro, M.; Sadow, A. D.; Huang, W.; Luijten, E.; Perras, F. A. Mechanistic Insights into Processive Polyethylene Hydrogenolysis through In Situ NMR. *Macromolecules* **2023**, *56*, 4287−4295.
(98) Dewis, L. I.; Rudrakshula, M.; Williams, C.; Chiarparin, E.; Myers, E. L.; Butts, C. P.; Aggarwal, V. K. Conformationally Controlled sp^3-Hydrocarbon-Based α-Helix Mimetics. *Angew. Chem., Int. Ed.* **2023**, *62*, No. e202301209.
(99) Fulmer, G. R.; Miller, A. J. M.; Sherden, N. H.; Gottlieb, H. E.; Nudelman, A.; Stoltz, B. M.; Bercaw, J. E.; Goldberg, K. I. NMR Chemical Shifts of Trace Impurities: Common Laboratory Solvents, Organics, and Gases in Deuterated Solvents Relevant to the Organometallic Chemist. *Organometallics* **2010**, *29*, 2176−2179.

https://doi.org/10.1021/acscatal.5c04494
ACS Catal. 2025, 15, 16924−16937